Journal of Luminescence 277 (2025) 120912

Contents lists available at ScienceDirect

Journal of Luminescence

journal homepage: www.elsevier.com/locate/jlumin

Full Length Article

Fluorescent gold nanoclusters stabilized by lysozyme: Synthesis and deposition kinetics on silica substrates

Julia Maciejewska-Prończuk [a,*], Magdalena Oćwieja [a], Paulina Żeliszewska [a], Monika Wasilewska [a], Ditta Ungor [b], Edit Csapó [b,c], Lilianna Szyk-Warszyńska [a], Marta Gajewska [d], Agnieszka Charzanowska [e], Joanna Dobrzyńska [f], Inna Ivashchenko [g], Katarzyna Matras-Postołek [g], Zbigniew Adamczyk [a]

[a] Jerzy Haber Institute of Catalysis and Surface Chemistry, Polish Academy of Sciences, Niezapominajek 8, PL-30239, Krakow, Poland
[b] Department of Physical Chemistry and Materials Science, University of Szeged, H-6720, Rerrich B. sqr. 1, Szeged, Hungary
[c] MTA-SZTE Biomimetic Systems Research Group, Department of Medical Chemistry, University of Szeged, H-6720, D' om sqr. 8, Szeged, Hungary
[d] AGH University of Science and Technology, Academic Centre for Materials and Nanotechnology, Mickiewicza 30, 30-059, Krakow, Poland
[e] Department of Physical Chemistry, Institute of Chemical Sciences, Faculty of Chemistry, Maria Curie-Sklodowska University in Lublin, M. Curie-Sklodowska Sq. 3, 20-031, Lublin, Poland
[f] Department of Analytical Chemistry, Institute of Chemical Sciences, Faculty of Chemistry, Maria Curie-Sklodowska University in Lublin, M. Curie-Sklodowska Sq. 3, 20-031, Lublin, Poland
[g] Cracow University of Technology, Faculty of Chemical Engineering and Technology, Warszawska 24, 31-155, Krakow, Poland

ARTICLE INFO

Keywords:
Fluorescent gold nanoclusters
Layered materials
Fluorescent layers
Self-assembly processes
Electrostatically-driven deposition
Lysozyme
QCM

ABSTRACT

Gold nanoclusters suspension were effectively synthesized under alkaline conditions in a chemical reduction process involving gold(III) chloride trihydrate and lysozyme (LYZ) molecules. Their size determined by high-resolution transmission electron microscopy (HR-TEM) was equal to 1.9 ± 0.5 nm. The nanoclusters, referred to as LYZ-Au NCs, were stable at pH below 4 and above 8, exhibiting a hydrodynamic diameter between 8 and 11 nm. The isoelectric point of LYZ-Au NCs appeared at pH 5.0. The suspension showed a pronounced fluorescence characterized by the red-emitting band at 668 nm. The deposition kinetics and stability of LYZ-Au NCs on bare and poly(diallyldimethylammonium chloride) (PDADMAC)-modified silica sensors were studied using quartz crystal microbalance (QCM). The influence of ionic strength, pH, and suspension concentration on the kinetics of LYZ-Au NCs deposition was determined. The significant increase in the maximum coverage of LYZ-Au NCs with ionic strength was attributed to the decreasing range of electrostatic interactions between deposited clusters. Atomic force microscopy (AFM) confirmed the formation of homogeneous layers of LYZ-Au NCs with controlled coverage on bare silica at pH 3.5 and PDADMAC-modified silica. It was shown by confocal microscopy investigations, that these layers also exhibited pronounced fluorescent properties.

1. Introduction

Fluorescent metal nanoclusters obtained on a protein matrix are characterized by large Stokes shifts, excellent photoluminescence, photostability, and low toxicity compared to quantum dots [1,2]. Thanks to these properties, they are widely used in genetic and cancer diagnostics, targeted drug delivery, catalysis, and chemical analysis [3,4].

Analogously, because of the abundance of binding sites, protein-stabilized clusters are often applied for sensing several biologically important or harmful cations/molecules [5–8]. For instance, Guo and Irudayaraj developed a procedure enabling the synthesis of bovine serum albumin-stabilized silver clusters (BSA-Ag NCs), which exhibited fluorescence emission at 637 nm [9]. It was found that those clusters were highly sensitive and selective in the detection of Hg^{2+}-ions, with a LOD (limit of detection) equal to 10 nM in the linear range from 10 nM to 5 μM [9]. Goswami et al. proved that blue-emitting copper clusters obtained with the use of BSA (BSA-Cu NCs) were excellent sensors for detecting Pb^{2+}-ions [10]. Transferrin, which belongs to plasma proteins and plays a critical role in iron homeostasis, was used for the preparation

* Corresponding author.
E-mail address: julia.maciejewska-pronczuk@ikifp.edu.pl (J. Maciejewska-Prończuk).

https://doi.org/10.1016/j.jlumin.2024.120912
Received 31 July 2024; Received in revised form 16 September 2024; Accepted 21 September 2024
Available online 24 September 2024

of gold (Tf-Au NCs) and copper nanoclusters (Tf-Cu NCs) [11,12]. Due to the ability of Tf to enter Tf receptor (TfR)-overexpressing cells, Tf-Cu NCs coupled with doxorubicin found application in targeted drug delivery systems [12].

A sensitive method aimed at the detection of ascorbic acid (AA), based on the oxidative etching effect of iodine (I_2) on lysozyme-stabilized silver nanoclusters (Lys-Ag NCs) with fluorescence quenching, was developed by Mo et al. [13]. Lysozyme also proved to be an excellent reagent for the synthesis of blue-emitting copper clusters (LYZ-Cu NCs), which, due to their negligible toxicity, have found application in cell labeling [3].

Chen and Tseng described the synthesis and application of red-emitting lysozyme-stabilized gold clusters (LYZ-Au NCs) for sensing glutathione in a single drop of blood [14]. The authors observed that LYZ-Au NCs can detect glutathione molecules through their core-etching process. It was established that the limit of detection at a signal-to-noise ratio of 3 for glutathione was equal to 20 nM [14]. LYZ-Au NCs turned out to be excellent detectors of copper ions. Shanmugaraj and Ilanchelian found that the emission intensity of LYZ-Au NCs, with an average size of 2.5 ± 0.3 nm, decreased linearly with the increasing concentration of Cu^{2+}-ions [15]. The limit of detection for Cu^{2+}-ions in the developed method was found to be 20 nM. Furthermore, LYZ-Au NCs exhibited good selectivity towards the detected ions even in the presence of a 100-fold higher concentration of common interfering cations [15].

The application of Au NCs prepared on lysozyme matrix (LYZ-Au NCs) for selective and specific recognition of the vitamin B6 cofactor pyridoxal-5′-phospahete (PLP) was described by Bothra et al. [16] and Upadhyay et al. [17]. The prepared PLP-LYZ-Au NCs conjugates was also applied for the selective turn-on recognition of Zn^{2+} ions in aqueous medium an living HeLa cells [16]. In turn, Bhardwaj et al. [18] also described the sensitive detection of Zn^{2+}-ions with the use of LYZ-Au NCs modified by salicylaldehyde (SA). The authors established that the probe SA_LYZ-Au NCs showed selective turn-on fluorescence enhancement at 452 nm due to the complexation-induced aggregation of the nanoclusters.

Among other examples of effective applications of protein-stabilized Au NCs, one can mention the utilization of human serum albumin-stabilized gold nanoclusters (HSA-Au NCs) for the detection and discrimination of *Staphylococcus aureus* and methicillin-resistant *Staphylococcus aureus* [19]. HSA-Au NCs were also employed in the development of a new fluorescence quenching-based non-enzymatic method for the sensitive and reliable detection of free bilirubin in blood serum [20]. It was also demonstrated that gamma globulin-stabilized Au NCs (γG-Au NCs) are effective probes for the fluorometric detection of inorganic pyrophosphate and pyrophosphatase [21] as well as tryptophan metabolites [22].

Au NCs with enhanced and tunable fluorescence are also widely applied as bioimaging probes and labels [2,4,23]. Numerous literature reports point out the promising applications of Au NCs for labeling biotin in cells, specifically staining the cell nucleus, monitoring cellular apoptosis, or *in vivo* self-imaging of tumors [24]. It is worth mentioning examples that have demonstrated the utility of functionalized BSA-Au NCs for *in vivo* imaging of mice tumors, detecting cancer cells with overexpressed folate receptors via fluorescence microscopy, or tracing pathways of tumor-targeted drug delivery systems [24].

Recently, much effort has been focused on investigations of the application of fluorescent Au NCs for *in vivo* imaging of neurodegenerative diseases such as Alzheimer's and Parkinson's diseases [25,26]. Firstly, it was established that Au NCs and Au NPs could penetrate the blood-brain barrier [26]. On the other hand, it was confirmed that Au NCs and Au NPs inhibit of protein fibrillization, which leads to the formation of numerous senile plaques responsible for neurodegenerative diseases [27–29]. For these reasons, fluorescent Au NCs can be inhibitors of neurodegenerative diseases and simultaneously bioimaging probes for tracking changes in diseased brain areas [25]. Therefore, the potential toxicity of protein-stabilized fluorescent metal clusters is the most significant issue for their effective biomedical application. Moreover, it is conceivable that due to the stabilization of the metallic core by proteins, such fluorescent metal clusters can exhibit similar properties and adsorption abilities as the pure proteins used for their synthesis.

However application range of nanoclusters, the knowledge of their physicochemical properties is still incomplete and ambigous. Therefore, this work was focused on determining the physicochemical properties of Au NCs synthesized on lysozyme scaffolds (LYZ-Au NCs). For diverse sensing applications and effective bioimaging, the changes in the hydrodynamic diameters of clusters and their electrokinetic properties are important. Similarly, the impact of pH and ionic strength-induced changes in the emission spectra should be precisely determined to improve their sensing properties. To the best of our knowledge, such a report has not been published. Analyzing the literature data, one can also notice that little is known about nanocluster self-organization processes at solid/liquid interfaces leading to layered structure formation. This knowledge is crucial for designing functional sensor films in two-dimensional systems.

Therefore, the main goal of this work was to determine the physicochemical properties of LYZ-Au NCs and the mechanism of their deposition on a bare and macroion modified silica surfaces. It was assumed that the self-assembly of LYZ-Au NCs can be controlled by electrostatic interactions. To verify this hypothesis and develop a quantitative description of the deposition processes, kinetic measurements are carried out by applying the *in situ* quartz crystal microbalance (QCM-D) method. The influence of ionic strength, pH on the maximum coverage and stability of LYZ-Au NCs layers is quantitatively determined. The topography of the layers is characterized by atomic force microscopy (AFM) and their fluorescent properties are acquired by confocal microscopy.

2. Materials and methods

2.1. Reagents

Lysozyme (LYZ) (crystallized and lyophilized powder, from chicken egg white), gold(III) chloride trihydrate, and sodium hydrochloride were obtained from Aldrich. Poly(diallyldimethylammonium chloride), hereafter referred to as PDADMAC, having the number averaged molar mass of 101,000 g mol^{-1} (101 kDa) was purchased from Polymer Standard Service GmbH, Germany. Other reagents such as sodium chloride, hydrochloric acid, sulphuric acid, and hydrogen peroxide were supplied by POCH S.A. (Avantor Performance Materials Poland). These chemicals were used without any further purification.

Ultrapure water (Milli-Q water) of specific conductivity 0.06 μS cm^{-1} was obtained using the Milli-Q Elix & Simplicity 185 purification system (Millipore SA Molsheim, France).

2.2. Synthesis of lysozyme-stabilized gold nanoclusters (LYZ-Au NCs)

Gold clusters stabilized by lysozyme (LYZ-Au NCs) were prepared according to a modified procedure of Hornok et al. [30]. Briefly, 83.6 mL of an aqueous solution of lysozyme (0.33 mmol L^{-1}) was mixed with 3.95 mL of a 25.4 mM gold (III) chloride solution. After 5 min of vigorous stirring of the mixture at ambient conditions, its pH was adjusted to 12 using a 1 M solution of sodium hydroxide. Then, the post-reaction mixture was maintained in a water bath at a temperature of 40°C for 24 h and then cooled to an ambient temperature. The nominal mass of the protein and gold in the mixture was equal to 400 mg and 20 mg, respectively.

Afterward, the suspension was purified from the excess ions originating from sodium hydroxide and the gold precursor using the ultrafiltration method. The process was carried out using an Amicon 8400 ultrafiltration chamber equipped with a regenerated cellulose membrane (Millipore, nominal molecular weight limit: 10 kDa) and Milli-Q water. The progress in purification was monitored by measuring the

specific conductivity and pH of the effluent solution. The cleaning procedure was terminated when the specific conductivity of the last fraction of the effluent solution decreased to 30 μS cm^{-1}. The volume of the suspension was then adjusted to 100 mL, which resulted in the nominal concentration of lysozyme and gold of 4000 mg L^{-1} and 200 mg L^{-1}, respectively. After the cleaning procedure, this stock LYZ-Au NC aqueous suspension was stored in a refrigerator at a temperature of 4°C.

2.3. Physicochemical characteristic of LYZ-Au NCs dispersed in suspensions

The concentration of gold in the samples of diluted LYZ-Au NC suspensions was determined using a Varian SpectraAA 800 atomic absorption spectrometer (AAS) equipped with a GTA 100 graphite furnace and Zeeman background correction. The temperature program used for determination was adjusted as follows: drying 120°C for 40 s, pyrolysis 500°C for 10 min, atomization 2600°C for 5 s. Briefly, controlled amounts of LYZ-Au NC suspension were mixed with 5 mL of hot aqua regia to dissolve the nanoclusters. The digestion time was 24 h. Subsequently, the mixtures were diluted with MilliQ water to a volume of 50 mL. The progress of LYZ-Au NC dissolution was evaluated using fluorescent measurements and dynamic light scattering technique (DLS).

The optical and fluorescence properties of LYZ-Au NCs were evaluated by measuring absorption and emission spectra. For this purpose, a UV-2600 spectrometer (Shimadzu) and a spectrofluorometer Quanta MasterTM 400 (Photon Technology International) were used. The spectra were recorded for suspensions with controlled concentration, pH, and ionic strength. The emission was excited at the maximum of the excitation band (at 380 nm). The spectra were recorded at room temperature using 10 mm quartz cells. For the calculation of the absolute internal quantum yield (QY %), the incident light spectra and both indirect and direct excitation were applied on the same apparatus equipped with the ABL&E JASCO ILF-835 integrating sphere in 2 mm optical length and 3 mm aperture. The registered spectra were corrected by using ABL&E JASCO ESC-842 calibrated WI light source, thus, other references were not needed. The calculations were done by the ABL&E JASCO SpectraManager 2.0 software of the instrument. The lifetime decay curves were recorded by time-correlated single photon counting (TCSPC) technique on a Horiba DeltaFlex device. The instrument was equipped with a DeltaDiode pulsed laser (λ_{laser} = 371 nm), and the samples were filled into a 1 cm quartz cuvette. The emitted light was detected at 660 nm with an 8 nm slit. The number of counts on the peak channel was 500 due to the long decay and the instrument response function (IRF) was measured by standard SiO_2 colloids (Horiba). The main lifetime components were calculated in the EZTime program of Horiba by the exponential fitting of decay curves and the goodness of fitting was characterized by χ^2 values.

The morphology and the average size of the metal part of LYZ-Au NCs were determined using high-resolution transmission electron microscopy (Tecnai TF 20 X-TWIN, FEI). Obtained micrographs were analysed using the MultiScan software provided by Computer Scanning System. A histogram was generated by measuring the surface area and diameter of 1000 metallic cores of LYZ-Au NCs. Additionally, the chemical composition of the samples was confirmed by energy dispersive spectroscopy (EDS).

The diffusion coefficient (D) of LYZ-Au NCs dispersed in the aqueous suspensions of controlled pH, ionic strength and temperature were measured using dynamic light scattering technique (DLS). Using these data, the hydrodynamic diameter (d_H) was calculated using the Stokes-Einstein relationship [31].

The electrophoretic mobility (μ_e) of LYZ-Au NC was acquired using the electrophoretic light scattering (ELS) technique. The zeta potential (ζ) was calculated from the Henry formula [32].

The DLS and ELS investigations were performed with the use of a Zetasizer Nano ZS (Malvern).

2.4. Preparation of LYZ-Au NC layers under flow transport conditions

The adsorption kinetics of LYZ-Au NCs on Si/SiO_2 Sensors (QSX 303), bare and functionalized by PDADMAC layers was investigated using a Qsense E1 quartz crystal microbalance with dissipation monitoring (QCM-D). Firstly, a stable baseline for the pure NaCl solution with controlled ionic strength and pH was obtained. In the case of functionalized sensors, after stabilizing the baseline, a compact PDADMAC layer was adsorbed. The adsorption was carried out over 15 min at pH 5.6 and an ionic strength of 10^{-2} M from solutions with the concentration of 5 mg L^{-1} at the flow rate of 1.33 x 10^{-3} cm^3 s^{-1}. After rinsing the PDADMAC functionalized sensor with NaCl solution of the same ionic strength, the deposition of LYZ-Au NCs was initiated by flushing the suspension through the cell at flow rates of 1.33 x 10^{-3} cm^3 s^{-1}. The concentration of LYZ-Au NC suspension varied between 5 and 15 mg L^{-1}. The ionic strength and pH of the suspensions were regulated using solutions of sodium hydroxide, hydrochloric acid, and sodium chloride. The deposition of LYZ-Au NCs was carried out for 30–180 min depending on the ionic strength and mass concentration of the suspension. Subsequently, the cell was rinsed with a sodium chloride solution of the same ionic strength and pH, and the stability of the obtained layers was determined. The temperature in all QCM-D experiments was kept at 25°C. The coverage of LYZ-Au NCs (Γ) was calculated from the formula [33]:

$$\Gamma = C_s(-\Delta f / n_0) \quad (1)$$

where Δf is the frequency shift, n_0 is the overtone number and C_s is the Sauerbrey's constant equal to 0.177 mg m^{-2} Hz^{-1} for the 5 MHz AT cut quartz sensor.

It should be noted that the coverage derived from QCM-D measurements significantly exceeds the actual mass coverage because it includes a contribution from hydrodynamic forces due to sensor oscillations [34, 35]. Therefore, to calculate the actual (often referred to as dry) coverage, a correction function is introduced. This function has been determined for various proteins, such as lysozyme [36], HSA [37], fibrinogen [38], and protein aggregates [39]. For a large protein coverage range, the correction function for proteins approaches 0.5, independently of the overtone number.

2.5. Physicochemical characteristic of LYZ-Au NC layers

The topography of LYZ-Au NC layers was determined by atomic force microscopy (AFM). The imaging of the layers was carried out using the NT-MDT Solver PRO device with the SMENA SFC050L scanning head. The measurements were performed in semi-contact mode using a silicon probe (polysilicon cantilevers with resonance frequencies of 240 kHz ±10 % or 140 kHz ±10 %, a typical tip curvature of 10 nm, and a cone angle less than 20°).

The fluorescence properties of the obtained LYZ-Au NC layers were examined using an inverted confocal laser scanning microscope (CLSM) (Zeiss, LSM780). The samples were observed using a 10 × Plan Apochromat objective with a numerical aperture of 0.45 and a magnification of 1 or 5. Si/SiO_2 sensors coated with LYZ-Au NC films were excited using a 10 % argon laser power of 30 mW at 355 nm.

3. Results and discussion

3.1. Physicochemical properties of LYZ-Au NCs in suspensions

The gold clusters stabilized by lysozyme, hereafter referred to as LYZ-Au NCs, were synthetized in the form of an aqueous suspensions according to the method described by Wei et al. [40], Hornok et al. [30], and Russell et al. [41]. However, in contrast to this protocol, after completing the synthesis, the LYZ-Au NCs suspension was thoroughly purified from the excess electrolyte. In this way, suspension

characterized by controlled ionic strength and pH of 8 was produced. Such precise purification of the LYZ-Au NC suspension is crucial for successful deposition experiments.

The AAS measurements conducted for the series of diluted suspensions revealed that the mass concentration of gold linearly increased with the mass concentration of LYZ (Supporting Materials, Fig. S1). This enabled to determine that the mass concentration of gold in the stock suspension of LYZ-Au NCs was equal to 178 ± 4 mg L^{-1}. Given that the nominal concentration of gold in the purified suspension was 200 mg L^{-1} one can calculate that 89 % of the gold initially present in the solution formed clusters. This conclusion is confirmed by an HR-TEM investigation (see Supporting materials Fig. S2), which showed that LYZ-Au NCs are composed of spherical gold cores averaging 1.9 ± 0.5 nm in size (Fig. 1a). For comparison, the gold core size reported by Wei et al. [40] and Hornok et al. [30] ranged from 1.1 to 1.5 nm. For comparison, the hydrodynamic diameter of LYZ molecules, derived from DLS measurements, was found to be 4 ± 1 nm [42].

Fig. 1b shows the extinction and fluorescence spectrum of diluted LYZ-Au NC suspension. Two characteristic bands occurring at the wavelengths of 221 and 280 nm in the absorption spectrum of LYZ-Au NCs were attributed to LYZ molecules. No other absorption bands were detected at higher wavelengths. This finding is consistent with the observations reported for clusters exhibiting a size of 1.5 nm [30,40]. Previously, it was established that no adsorption peaks appear in the visible region because protein-stabilized Au NCs are too small to exhibit localized surface plasmon resonance (LSPR) [30]. It is also worth mentioning that no sharper and more intense plasmon absorption band with the peak at 525 nm was observed for 3 and 4 nm-sized Au NCs stabilized by thioether-terminated polymeric stabilizers [43].

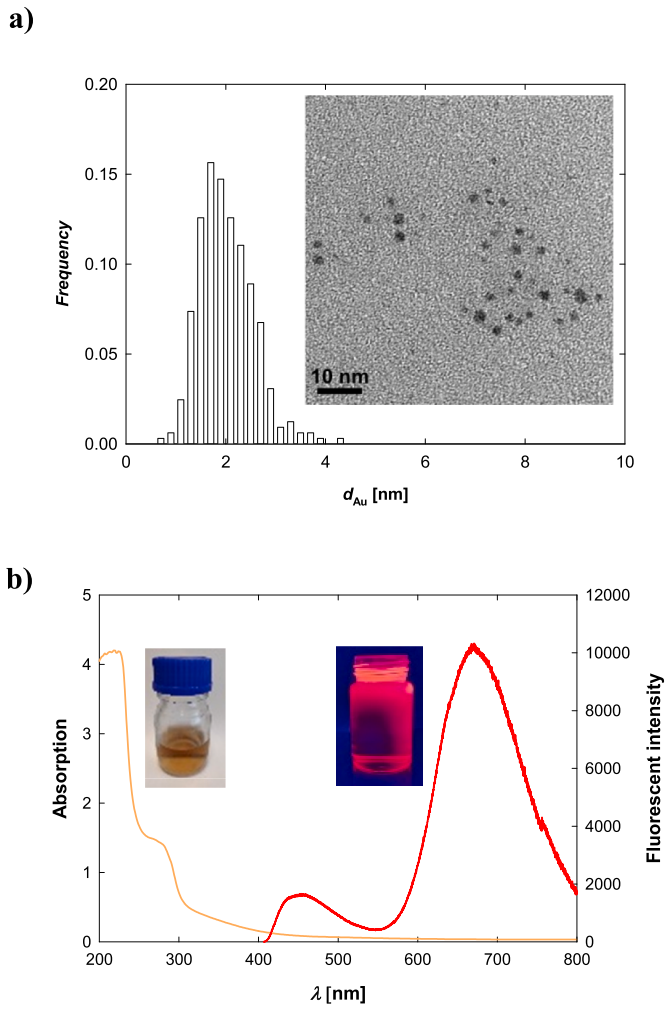

Fig. 1. a) Typical TEM micrograph presenting gold cores of LYZ-Au NCs and their size distribution. **b)** Absorption (orange) and emission (red) spectra of LYZ-Au NCs dispersed in the stock suspension at pH 8.0 (LYZ concentration: 500 mg L^{-1}, Au concentration: 22.3 mg L^{-1}). The excitation wavelength was 380 nm. The insets show images of LYZ-Au NC suspension in daylight and under UV irradiation.

It should be underlined that despite the relatively larger size of the gold cores, LYZ-Au NCs suspension exhibited excellent fluorescence properties. The average internal quantum yield is 3.8 %, while the average fluorescence lifetime is 1.9 μs. The emission spectrum of LYZ-Au NCs displays two characteristic peaks occurring at wavelengths of 448 nm and 668 nm (Fig. 1b). It is worth mentioning that these emission bands are bathochromically shifted compared to the bands detected for lysozyme-capped Au NCs with sizes of 1.0–1.5 nm [30,40,44]. However, Baksi et al. [45] demonstrated that the emission peak position of Au NCs prepared on the LYZ scaffold can also vary from 675 to 686 nm. It is worth mentioning that Wei et al. [40], in the first article reported successful synthesis of LYZ-Au NCs, established the occurrence of two characteristic bands in the emission spectra of the nanoclusters. The peaks were centered at 445 nm and 657 nm [40], which were slightly hypsochromically shifted compared to the positions of the peaks described in this report. To assign the emission peaks, Wei et al. conducted kinetic studies [40]. Based on the time-dependent fluorescence spectra of LYZ-Au NCs and the corresponding fluorescence intensity-reaction time curves, they detected that the peak occurring at a wavelength of 445 nm is due to a lysozyme-$HAuCl_4$ reaction intermediate, prior to the formation of the final LYZ-Au NCs. Numerous subsequent scientific reports on LYZ-Au NCs have confirmed the presence of these two characteristic bands.

In general, published results indicate that NIR-emitting protein-Au NCs typically exhibit two excitation maxima ($\lambda_{ex.}$ max at 370 nm and 510 nm) and one emission maximum in the NIR region ($\lambda_{em.}$ max at 650–670 nm) [46]. They have a higher quantum yield of 6% compared to their monolayer-protected counterparts [46]. Upon excitation at 370 nm, emission around 450 nm is observed. This emission is attributed to either the protein's intrinsic fluorescence by some groups or to Au_8 by others [46]. It is worth mentioning that the position of these two bands depends on the structural properties of the formed clusters, such as the number of atoms in the gold core and structural changes in the lysozyme molecules.

Extensive investigations were also conducted in this work to determine the influence of ionic strength and pH on the optical properties of LYZ-Au NCs under various physicochemical conditions, comprising the extinction and emission spectra. The results of these measurements carried out at ionic strengths of 10^{-4}, 10^{-3}, 10^{-2}, and 0.15 M are shown in Supporting Materials (Fig. S3 and Fig. S4).

The absorption spectra showed two bands at 221 and 280 nm pertinent to LYZ molecules. On the other hand, the characteristic absorption band of gold nanoparticles at 530 nm was not detected in the extinction spectrum (Fig. S3). This is consistent with the basic principles [47] and the observation by Hussain et al. [43] that the sharp and intense plasmon absorption band near 525 nm in the extinction spectrum is characteristic of AuNPs with the size above 5 nm.

The increase in absorbance at 221 and 280 nm wavelengths is particularly well noticeable in spectra recorded at larger ionic strengths (Supporting Materials, Fig. S3). Moreover, the absorption of LYZ-Au NCs over the entire range of wavelengths significantly increases at pH in the range of 4–7. This effect was independent of ionic strength. These results are consistent with the reports of Russell et al. [41], who confirmed an increase in the absorption of LYZ-stabilized Au NCs between pH 3 and 6, albeit without considering the effect of ionic strength.

The analysis of emission spectra also confirmed a significant influence of pH and ionic strength on the fluorescence properties of LYZ-Au NCs (Supporting Materials, Fig. S4). The largest intensity of emission bands at wavelengths of 448 and 668 nm was observed at pH 5.0,

independently of ionic strength. For ionic strengths of 10^{-3} M and 10^{-2} M, the emission intensity at pH 8 and 9 was comparable to that observed at pH 4. Under acidic conditions, LYZ-Au NCs exhibited the lowest fluorescence. It was established that at pH 4, the intensity of the emission band at 668 nm systematically decreased with the increase in ionic strength. This indicates that both the optical properties and fluorescence of LYZ-Au NCs could be controlled by the pH and ionic strength of their solutions.

To quantitatively characterize the size of the nanoclusters and the stability of LYZ-Au NCs suspensions for various pHs and ionic strengths, DLS measurements were carried out according to the above described procedure. The hydrodynamic diameter of LYZ-Au NCs determined for the stock suspension (pH 8.0) was equal to 6 ± 4 nm. It is worth mentioning that the hydrodynamic diameter of LYZ-stabilized Au NCs reported by Lin and Tseng [48] as well as Russell et al. [41] was equal to 8 ± 2 nm. On the other hand, Ungor et al. [44] reported the value of the cluster size 5 ± 1 nm (at pH 7.4 and ionic strength 10^{-2} M), whereas Hornok et al. [30] showed that their hydrodynamic diameters varied from 4 ± 1 nm to 6 ± 2 nm depending on the preparation conditions.

In Fig. 2a, the dependence of the hydrodynamic diameter of the purified LYZ-Au NCs on pH, for various ionic strengths is presented. At ionic strength of 10^{-2} M, the hydrodynamic diameter was equal to 8 ± 2 and 11 ± 2 nm at pH of 2 and 4, respectively. Similar hydrodynamic diameter values were determined for pH above 7. Between pH 4.0 and 7.0, there is a significant increase in the hydrodynamic diameters,

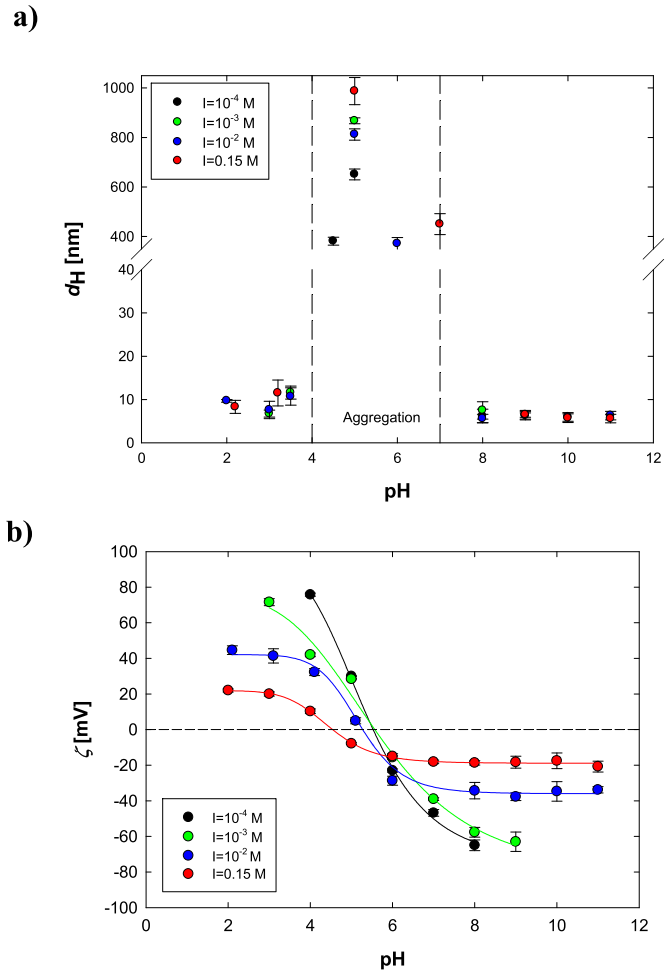

Fig. 2. Dependence of LYZ–Au NC **a)** hydrodynamic diameter and **b)** zeta potential on pH determined for various ionic strengths. The measurements were conducted at $T = 25$°C and for LYZ and Au concentrations equal to 500 mg L^{-1} and 22 mg L^{-1}, respectively. Solid lines are guides for the eyes.

indicating aggregation of LYZ-Au NCs. At ionic strength of 0.15 M, LYZ-Au NC aggregates with hydrodynamic diameter above 400 nm appear at pH ranging from 3.5 to 8.0. This effect correlates with the observation of Russell et al. [41], who confirmed the formation of aggregates of LYZ-stabilized Au NC within the pH range of 3–5.

It is worth mentioning that the stability of colloidal systems, such as LYZ-Au NCs, can be considered in different ways. Regarding their fluorescent properties, it can be stated that they are unstable when fluorescence quenching occurs, for example, in the presence of mercury ions. This relationship has been described in literature reports [2,4]. The stability of LYZ-Au NCs can also be considered in terms of structural changes occurring in one of the components, such as when the metallic core is digested. In this case, the digestion of the Au NC core results in the loss of fluorescent properties. In another scenario, due to a decrease in repulsive interactions induced by an increase in ionic strength or changes in pH, the individual clusters could agglomerate or aggregate into larger nano- or macrostructures. This effect is detectable by an increase in the hydrodynamic diameter of the nanoclusters which was present in Fig. 2a. Nevertheless, these structural changes in the system do not lead to fluorescence quenching. In this case, the electrostatically-driven aggregation causes an increase in the intensity of characteristic emission bands, as shown in the Supporting Materials, Fig. S4. This phenomenon is well-described in the literature as aggregation-enhanced emission (AIE) [49–52].

The strongest fluorescence of LYZ-Au NCs observed at pH 5.0 independently on ionic strength (Fig. S4 Supporting materials) results from AIE. Xie et al. first reported the aggregation-induced emission (AIE) of metal nanoclusters in 2012 [49], although the concept of this effect was proposed by Tang et al., in 2001 for fluorescent polymers [50]. This effect in gold nanoclusters is well-known and described in the literature [51,52], however the impact of ionic strength on AIE has not been reported before.

In the next stage of research, the electrophoretic mobility of LYZ-Au NCs was determined using Lased Doppler Velocimetry (LDV). Knowing the values of electrophoretic mobility (Supporting materials, Table S1), the zeta potential was calculated using the Henry's formula. The zeta potential of the nanoclusters was equal to −65 ± 3 mV (pH 8.0). Lin and Tseng [48] reported that the zeta potential of such clusters amounted to 38 ± 2 mV. In contrast, Honrok et al. [30] showed that the zeta potential of protein-stabilized AuNPs exhibited a negative zeta potential, ranging from −21 mV to −30 mV, whereas for Au NCs, the zeta potential was about −15 mV. Unfortunately, ionic strength and pH of these measurements were not specified in these works.

Fig. 2b shows the dependence of the zeta potential of LYZ-Au NCs on pH at various ionic strengths. It can be noticed that for a given ionic strength, the zeta potential is positive at the range pH 3 to 5 and negative otherwise. This suggests that the LYZ-Au NCs exhibit an apparent isoelectric point at pH about 5. For comparison, Russel et al. [41] showed that his LYZ-Au NCs exhibited the isoelectric point at pH 4.

One can also see in Fig. 2b that at a given pH, the zeta potential is dependent on ionic strength. For example, at pH 4.0 the zeta potential is equal to 75 ± 1 and 42 ± 1 mV for ionic strength 10^{-4} M and 10^{-3} M, respectively, whereas at ionic strength of 0.15 M, it decreased to 10 ± 2 mV. Analogous dependencies appear under alkaline conditions. Thus, at pH 9.0 the zeta potential is equal to −63 ± 5 and −18 ± 3 mV at an ionic strength of 10^{-3} M and 0.15 M, respectively. Generally, the increase in ionic strength caused a pronounced decrease in the absolute value of the zeta potential of LYZ-Au NCs.

Considering the above DLS and ELS results, one can argue that the significant shift in the isoelectric point of LYZ-Au NCs to acidic pHs compared to the isoelectric point of LYZ molecules can be attributed to the protein aggregation rather than to the binding of the gold cores to the protein molecules. This hypothesis was validated by performing additional investigations where the pure LYZ solution with pH adjusted to 12 was heated over 24 h. Afterward, the solution was purified according to the same procedure applied for LYZ-Au NCs. Subsequently,

the electrokinetic properties of the LYZ molecule were determined. The results of these investigations, presented in Fig. S5 (Supporting materials), indicate that the isoelectric point of the treated LYZ molecules was shifted to 5.8, compared to the isoelectric of 11 pertinent to native LYZ molecules [41].

The conclusion that the shift in the isoelectric point of LYZ-Au NCs is caused by protein aggregation is also supported if one considers that the mass concentration of gold derived from AAS is about 22 times smaller than the LYZ molecule mass. Considering that the size of the cores is 1.9 nm and the gold density is equal to 19.3 g cm^{-3} one can predict that the number concentration ratio of the cores to LYZ molecules is equal to 1/60, which means that less than 2 % of the LYZ molecules can form a complex with the metal core.

The above results enabled to establish that the LYZ-Au NCs are stable at pH below 4.0 and above 8.0 at ionic strengths below 0.15 M. It was also confirmed that the electrokinetic properties of LYZ-Au NCs can be tuned by ionic strength under acidic and alkaline conditions. These findings are crucial for selecting appropriate experimental conditions aimed at the formation of LYZ-Au NCs layers at Si/SiO_2 substrates.

4. Deposition kinetics of LYZ-Au NCs on Si/SiO_2 surfaces

The formation of LYZ-Au NC layers under controlled pH, ionic strength, temperature, and bulk concentration of suspensions was investigated *in situ* by QCM-D according to the above described procedure. The Si/SiO_2 sensors used in these investigations exhibited a negative zeta potential over a wide range of pH and ionic strength [53]. Therefore, to ensure effective adsorption of LYZ-Au NCs for pH above five where they exhibit a negative zeta potential (see Fig. 2b) the sensors were functionalized by PDADMAC, a strong cationic macroion [54] as above described.

Typical adsorption kinetics of PDADMAC on bare Si/SiO_2 surface is presented in the Supporting materials (Fig. S6). After the formation of a dense PDADMAC layer, its stability was assessed by rinsing the QCM-D cell with the PDADMAC-modified Si/SiO_2 sensor with a 10^{-2} M solution of NaCl at pH 5.6. No decrease in the mass of deposited PDADMAC was observed, confirming the stability of PDADMAC layers on Si/SiO_2 sensors under the investigated conditions (Supporting materials, Fig. S6).

The bare and PDADMAC-functionalized sensors were used for thorough kinetic investigations carried out under different pHs and ionic strength. The results obtained for the bare sensor at pH 3.5, flow rate of 1.33 x 10^{-3} cm^3 s^{-1} and various ionic strengths are shown in Fig. 3 as the dependence of the mass coverage Γ on the adsorption time. It should be mentioned that the coverage obtained from QCM-D using Eq. (1) was practically independent of the overtone number (Supporting Information).

As can be observed, the coverage abruptly increases with time and then stabilizes at a constant level, which is dependent on ionic strength. These plateau values, practically did not change upon initiating the desorption procedure where the pure electrolyte was flushed through the cell at the same rate and ionic strength. These coverages after the desorption were equal to 3.0, and 1.5 mg m^{-2} for ionic strength of 10^{-2} and 3.3 x 10^{-4} M, respectively. Considering the above correction function of 0.5, one can predict that these values correspond to the real LYZ-Au NC coverages of 1.5 and 0.75 mg m^{-2}, respectively.

It should be remembered that as shown above, LYZ-Au NCs are composed of Au cores and LYZ aggregates. However, for our sample the gold core to protein mass concentration ratio was only 0.046, irrespectively of the dilution degree. This indicates that the signal derived from the QCM-D kinetic measurements was mainly due to the protein adsorption.

The significant decrease in the maximum coverage of LYZ-Au NC can be attributed to the increased range of the repulsive electrostatic interactions among adsorbed molecules, which was observed for other proteins [55]. For comparison, the coverage of albumin at ionic strength of 1.3 x 10^{-3} and 10^{-2} M, was determined to be 0.42 and 0.66 mg m^{-2}, respectively [56]. Given that the maximum coverage of globular proteins monotonically increases with their molar mass (for spherically shaped molecules the scaling law is $M_w^{1/3}$), this comparison suggests that the protein aggregates in the LYZ-Au NCs were significantly larger than the albumin molecules, whose hydrodynamic diameter was equal to 7.5 nm [57]. This agrees with the above estimate of the hydrodynamic diameter of LYZ-Au NCs derived from DLS measurements, of 8–11 nm.

The significant role of electrostatic interactions is well illustrated in Fig. 4 where the LYZ-Au NCs coverage systematically increased with ionic strength, which was stepwise increased from 3.3 x 10^{-4} to 10^{-2} M.

The comparison of the results obtained for the bare and PDADMAC-functionalized sensor at pH 9 is presented in Fig. 5. As can be observed, the plateau coverage of LYZ-Au NC for the bare sensor only attained 0.5 mg m^{-2} and significantly decreased to 0.2 mg m^{-2} upon performing the desorption step. In contrast, for the functionalized sensor, the coverage stabilized after the desorption at the much larger value of 4.5 mg m^{-2} (for ionic strength of 10^{-2} M) which confirms more efficient adsorption of LYZ-Au NC. Analogously as for the bare sensor, the LYZ-Au NC coverage at the PDADMAC decreased for lower ionic strength, which

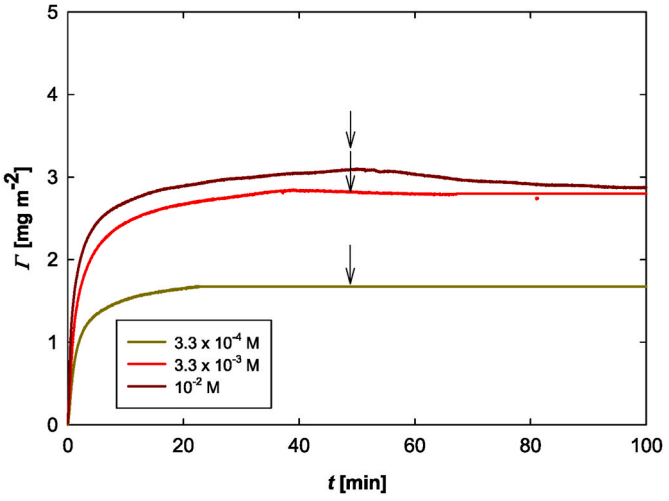

Fig. 3. The kinetics of LYZ-Au NC deposition on bare Si/SiO_2 sensor at pH 3.5 flow rate 1.33 x 10^{-3} cm^3 s^{-1}, the bulk concentration of 10 mg L^{-1}, for ionic strength 10^{-2} M (dark red line), 3.3 x 10^{-3} M (red line), 3.3 x 10^{-4} M (green line). The arrows show the beginning of the desorption runs.

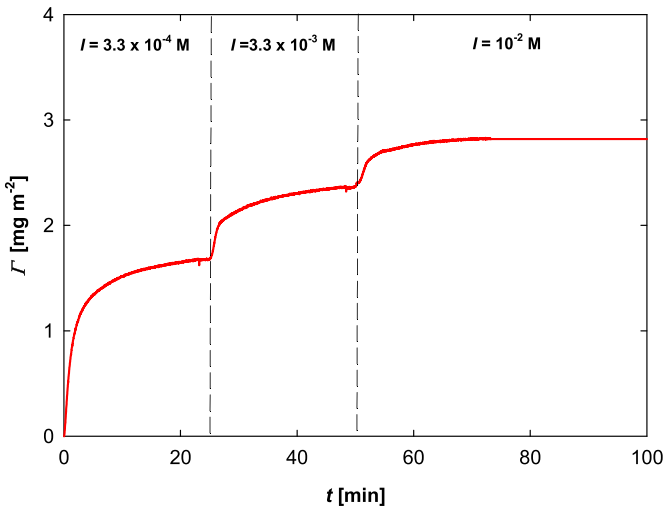

Fig. 4. The kinetics of LYZ-Au NC adsorption on bare Si/SiO_2 sensor; pH 3.5, flow rate 1.33 x 10^{-3} cm^3 s^{-1}, bulk concentration of 10 mg L^{-1}. Ionic strength was stepwise increased from 3.3 x 10^{-4} to 10^{-2} M.

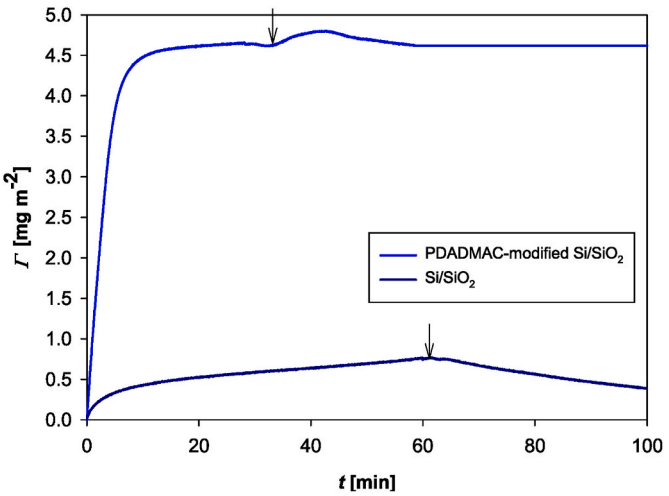

Fig. 5. The kinetics of LYZ-Au NC adsorption on PDADMAC-functionalized (blue line) and bare Si/SiO_2 sensor (dark blue line); pH 9; ionic strength 10^{-2} M, flow rate 1.33 x 10^{-3} cm^3 s^{-1}, bulk concentration of 10 mg L^{-1}, the arrows show the beginning of the desorption runs.

also confirms a significant influence of the electrostatic interactions among adsorbed molecules (see Suporting Materials, Fig. S7).

The deposition of LYZ-Au NCs on bare and PDADMAC-functionalized sensors was also carried out for various suspension concentrations under acidic and alkaline conditions. The results of these investigations are presented in Fig. S7 (Supporting materials). It was observed that in both cases the adsorption kinetics was proportional to the bulk suspension concentration. It is interesting to mention that analogous relationships were reported for both negatively charged [33] and positively charged [31] gold nanoparticles. This fact supports the hypothesis that the deposition of LYZ-Au NCs under flow conditions is primarily controlled by bulk transport.

The topography of LYZ-Au NC layers on Si/SiO_2 sensors was determined from atomic force microscopy (AFM) images. The results, shown in Fig. S8 (Supporting Materials), showed that the layers prepared on bare and PDADMAC-modified sensors under acidic and basic conditions exhibited a homogeneous structure. However, individual gold cores were not visible on AFM images due to their small size.

Gold nanoclusters exhibit fluorescence in the visible and near infrared range, but it is usually inefficient and strongly dependent on the structure of the nanocluster. In systems where nanoclusters are stabilized with ligands, e.g. lysozyme, the optical properties of the nanoparticles are enhanced by the ligand, resulting in an increase of the fluorescence efficiency. Since the LYZ-Au NC are too small to be visible under fluorescence microscopy, the quenching fluorescence phenomenon was used for observation under confocal microscopy to demonstrate the fluorescence properties of thin LYZ-Au NC layers deposited on bare and PDADMAC-modified sensors. The LYZ-Au NC layers were excited at a wavelength of 355 nm and imaged by confocal microscopy in the wavelength range of 600–670 nm. The results are shown in Fig. 6. To be sure that the observed light, is not just the background, but comes from the NCs, the small region of interest was selected and illuminated with the high laser intensity to photobleach the NCs. Next the power of laser was reduced to the primary value to take the LYZ-Au NC image. In the area illuminated by high laser intensity, the dark region due to quenching was visible, confirming the presence of LYZ-Au NCs on bare Si/SiO_2 surface. The same result was observed for LYZ-Au NCs on the PDADMAC modified Si/SiO_2 surface.

5. Conclusions

LYZ-Au NCs in the form of aqueous suspensions were effectively synthetized in a chemical reduction process involving gold(III) chloride acid and lysozyme molecule under alkaline conditions. The isoelectric point appeared at pH 5.0, compared to the isoelectric point of lysozyme (LYZ) reported to appear at pH of 11. This was attributed to the aggregation of protein molecules under synthesis conditions.

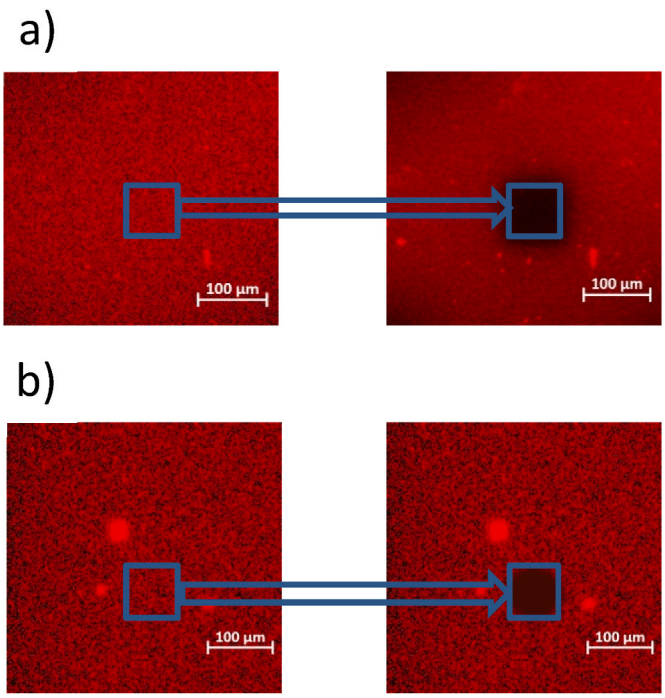

Fig. 6. Typical confocal laser scanning microscope images presenting the fluorescence properties of the LYZ-Au NC layers deposited on **a)** bare Si/SiO_2 surface at pH 3.5 and **b)** PDADMAC-modified Si/SiO_2 surface at pH 9.0.

The suspensions exhibited pronounced fluorescence properties with a characteristic emission band at a wavelength of 668 nm. It was also established that the emission properties of the solutions were pH and ionic strength-dependent.

The kinetics of self-assembly of LYZ-Au NCs on bare and PDADMAC-modified surfaces was quantitatively determined by QCM-D investigations. The significant increase in the maximum coverage of LYZ-Au NCs with ionic strength observed in these measurements was attributed to the decreasing range of electrostatic interactions among deposited clusters. Atomic force microscopy (AFM) confirmed the formation of homogeneous layers of LYZ-Au NCs with controlled coverage on negatively and positively charged surfaces. Confocal microscopy imaging showed that the deposited LYZ-Au NC layers exhibit pronounced fluorescence properties.

Our investigations confirmed that one can prepare homogeneous and stable LYZ-Au NCs layers exhibiting fluorescent properties whose coverage can be controlled by ionic strength, pH and deposition time.

CRediT authorship contribution statement

Julia Maciejewska-Prończuk: Writing – review & editing, Writing – original draft, Methodology, Investigation, Funding acquisition, Data curation, Conceptualization. **Magdalena Oćwieja:** Writing – review & editing, Writing – original draft, Investigation, Conceptualization. **Paulina Żeliszewska:** Methodology, Investigation. **Monika Wasilewska:** Writing – review & editing, Methodology, Investigation. **Ditta Ungor:** Writing – review & editing, Methodology, Investigation. **Edit Csapó:** Writing – review & editing, Methodology. **Lilianna Szyk-Warszyńska:** Investigation. **Marta Gajewska:** Investigation. **Agnieszka Charzanowska:** Investigation. **Joanna Dobrzyńska:** Investigation. **Inna Ivashchenko:** Investigation. **Katarzyna Matras-**

Postołek: Investigation. **Zbigniew Adamczyk:** Writing – review & editing, Supervision.

Declaration of competing interest

The authors declare that they have no known competing financial interests or personal relationships that could have appeared to influence the work reported in this paper.

Data availability

Data will be made available on request.

Acknowledgments

This research was funded by the National Science Centre (NCN) in Poland under the project Miniatura-5 No. 2021/05/X/ST5/00244.

Appendix A. Supplementary data

Supplementary data to this article can be found online at doi: mmcdoino

References

[1] L. Shang, S. Dong, G.U. Nienhaus, Ultra-small fluorescent metal nanoclusters: synthesis and biological applications, Nano Today 6 (4) (2011) 401–418, https://doi.org/10.1016/j.nantod.2011.06.004.
[2] L. Yang, P. Hou, J. Wei, B. Li, A. Gao, Z. Yuan, Recent advances in gold nanocluster-based biosensing and therapy: a review, Molecules 29 (7) (2024) 1574, https://doi.org/10.3390/molecules29071574.
[3] R. Ghosh, A.K. Sahoo, S.S. Ghosh, A. Paul, A. Chattopadhyay, Blue-emitting copper nanoclusters synthesized in the presence of lysozyme as candidates for cell labeling, ACS applied materials & interfaces 6 (6) (2014) 3822–3828, https://doi.org/10.1021/am500040t.
[4] J. Qiu, F. Ahmad, J. Ma, Y. Sun, Y. Liu, Y. Xiao, L. Xu, T. Shu, X. Zhang, From synthesis to applications of biomolecule-protected luminescent gold nanoclusters, Anal. Bioanal. Chem. 416 (2024) 3923–3944, https://doi.org/10.1007/s00216-024-05303-y.
[5] B. Hemmateenejad, F. Shakerizadeh-Shirazi, F. Samari, BSA-modified gold nanoclusters for sensing of folic acid, Sensors Actuators B Chem. 199 (2014) 42–46, https://doi.org/10.1016/j.snb.2014.03.075.
[6] X. You, Y. Li, Direct chemiluminescence of fluorescent gold nanoclusters with classic oxidants for hydrogen peroxide sensing, Arab. J. Chem. 12 (1) (2014) 69–74, https://doi.org/10.1016/j.arabjc.2015.05.019.
[7] X.-J. Li, J. Ling, C.-L. Han, L.-Q. Chen, Q.-E. Cao, Z.-T. Ding, Chicken egg white-stabilized Au nanoclusters for selective and sensitive detection of Hg(II), Anal. Sci. 33 (6) (2017) 671–675, https://doi.org/10.2116/analsci.33.671.
[8] M. Shellaiah, K. Sun, Luminescent metal nanoclusters for potential chemosensor applications, Chemosensors 5 (4) (2017) 36, https://doi.org/10.3390/chemosensors5040036.
[9] C. Guo, J. Irudayaraj, Fluorescent Ag clusters via a protein-directed approach as a Hg (II) ion sensor, Anal. Chem. 83 (8) (2011) 2883–2889, https://doi.org/10.1021/ac1032403.
[10] N. Goswami, A. Giri, M.S. Bootharaju, P.L. Xavier, T. Pradeep, S.K. Pal, Copper quantum clusters in protein matrix: potential sensor of Pb2+ ion, Anal. Chem. 83 (24) (2011) 9676–9680, https://doi.org/10.1021/ac202610e.
[11] X. Le Guével, N. Daum, M. Schneider, Synthesis and characterization of human transferrin-stabilized gold nanoclusters, Nanotechnology 22 (27) (2011) 275103, https://doi.org/10.1088/0957-4484/22/27/275103.
[12] U. Goswami, A. Dutta, A. Raza, R. Kandimalla, S. Kalita, S.S. Ghosh, A. Chattopadhyay, Transferrin–copper nanocluster–doxorubicin nanoparticles as targeted theranostic cancer Nanodrug, ACS Appl. Mater. Interfaces 10 (4) (2018) 3282–3294, https://doi.org/10.1021/acsami.7b15165.
[13] Q. Mo, F. Liu, J. Gao, M. Zhao, N. Shao, Fluorescent sensing of ascorbic acid based on iodine induced oxidative etching and aggregation of lysozyme-templated silver nanoclusters, Anal. Chim. Acta 1003 (2018) 49–55, https://doi.org/10.1016/j.aca.2017.11.068.
[14] T.-H. Chen, W.-L. Tseng, (Lysozyme Type VI)-stabilized Au_8 clusters: synthesis mechanism and application for sensing Glutathione in a single drop of blood, Small 8 (12) (2012) 1912–1919, https://doi.org/10.1002/smll.201102741.
[15] K. Shanmugaraj, M. Ilanchelian, A "turn off' fluorescent sensor for the selective and sensitive detection of copper(II) ions using lysozyme stabilized gold nanoclusters, RCS RSC Advances 6 (59) (2016) 54518–54524, https://doi.org/10.1039/C6RA08325K.
[16] S. Bothra, L.T. Babu, P. Paira, S.K. Ashok Kumar, R. Kumar, S.K. Sahoo, A biomimetic approach to conjugate vitamin B 6 cofactor with the lysozyme cocooned fluorescent AuNCs and its application in turn-on sensing of zinc (II) in environmental and biological samples, Anal. Bioanal. Chem. 410 (2018) 201–210, https://doi.org/10.1007/s00216-017-0710-2.
[17] Y. Upadhyay, R. Kumar, S.K. Sahoo, Developing a cost-effective bioassay to detect alkaline phosphatase activity and generating white light emission from a single nano-assembly by conjugating vitamin B6 cofactors with lysozyme-stabilized fluorescent gold nanoclusters, ACS Sustain. Chem. Eng. 8 (10) (2020) 4107–4113, https://doi.org/10.1021/acssuschemeng.9b06563.
[18] V. Bhardwaj, T. Anand, H.J. Choi, S.K. Sahoo, Sensing of Zn (II) and nitroaromatics using salicylaldehyde conjugated lysozyme-stabilized fluorescent gold nanoclusters, Microchem. J. 151 (2019) 104227, https://doi.org/10.1016/j.microc.2019.104227.
[19] P.-H. Chan, Y.-C. Chen, Human serum albumine stabilized gold nanoclusters as selective luminescent probes for *Staphylococcus aureus* and methicillin-resistant *Staphylococcus aureus*, Anal. Chem. 84 (21) (2012) 8952–8956, https://doi.org/10.1021/ac302417k.
[20] M. Santhosh, S.R. Chinnadayyala, A. Kakoti, P. Goswami, Selective and sensitive detection of free bilirubin in blood serum using human serum albumin stabilized gold nanoclusters as fluorometric and colorimetric probe, Biosens. Bioelectron. 59 (2014) 370–376, https://doi.org/10.1016/j.bios.2014.04.003.
[21] S. Xu, X. Feng, T. Gao, R. Wang, Y. Mao, J. Lin, X. Yu, X. Luo, A novel dual-functional biosensor for fluorometric detection of inorganic pyrophosphate and pyrophosphatase activity based on globulin stabilized gold nanoclusters, Anal. Chim. Acta 958 (2017) 22–29, https://doi.org/10.1016/j.aca.2016.12.026.
[22] D. Ungor, K. Horváth, I. Dékány, E. Csapó, Red-emitting gold nanoclusters for rapid fluorescence sensing of tryptophan metabolites, Sensor. Actuator. B Chem. 288 (2019) 728–733, https://doi.org/10.1016/j.snb.2019.03.026.
[23] M.I. Halawa, J. Lai, G. Xu, Gold nanoclusters: synthetic strategies and recent advances in fluorescent sensing, Materials Today Nano 3 (2018) 9–27, https://doi.org/10.1016/j.mtnano.2018.11.001.
[24] S. Palmal, N.R. Jana, Gold nanoclusters with enhanced tunable fluorescence as bioimaging probes, Wiley Interdisciplinary Reviews: Nanomedicine and Nanobiotechnology 6 (1) (2014) 102–110, https://doi.org/10.1002/wnan.1245.
[25] L. Lai, C. Zhao, X. Li, X. Liu, H. Jiang, M. Selke, X. Wang, Fluorescent gold nanoclusters for in vivo target imaging of Alzheimer's disease, RSC Adv. 6 (36) (2016) 30081–30088, https://doi.org/10.1039/C6RA01027J.
[26] J. Hu, G. Gao, M. He, Q. Yin, X. Gao, H. Xu, T. Sun, Optimal route of gold nanoclusters administration in mice targeting Parkinson's disease, Nanomedicine (2019) 15, https://doi.org/10.2217/nnm-2019-0268.
[27] J. Geng, K. Qu, J. Ren, X. Qu, Rapid and efficient screening of Alzheimer's disease β-amyloid inhibitors using label-free gold nanoparticles, Mol. Biosyst. 6 (2010) 2389–2391, https://doi.org/10.1039/C0MB00057D.
[28] Y.H. Liao, Y.J. Chang, Y. Yoshiike, Y.C. Chang, Y.R. Chen, Negatively charged gold nanoparticles inhibit Alzheimer's amyloid-β fibrillization, induce fibril dissociation, and mitigate neurotoxicity, Small 8 (2012) 3631–3639, https://doi.org/10.1002/smll.201201068.
[29] S. Hsieh, C.W. Chang, H.H. Chou, Gold nanoparticles as amyloid-like fibrillogenesis inhibitors, Colloids Surf. B Biointerfaces 112 (2013) 525–529, https://doi.org/10.1016/j.colsurfb.2013.08.029.
[30] V. Hornok, E. Csapó, N. Varga, D. Ungor, D. Sebők, L. Janovák, G. Laczkó, I. Dékány, Controlled syntheses and structural characterization of plasmonic and red-emitting gold/lysozyme nanohybrid dispersions, Colloid Polym. Sci. 294 (1) (2016) 49–58, https://doi.org/10.1007/s00396-015-3781-7.
[31] M. Oćwieja, J. Maciejewska-Prończuk, Z. Adamczyk, M. Roman, Formation of positively charged gold nanoparticle monolayers on silica sensors, J. Colloid Interface Sci. 501 (2017) 192–201, https://doi.org/10.1016/j.jcis.2017.04.038.
[32] M. Morga, Z. Adamczyk, S. Gödrich, M. Oćwieja, G. Papastavrou, Monolayers of poly-l-lysine on mica–Electrokinetic characteristics, J. Colloid Interface Sci. 456 (2015) 116–124, https://doi.org/10.1016/j.jcis.2015.05.044.
[33] K. Kubiak, Z. Adamczyk, J. Maciejewska, M. Oćwieja, Gold nanoparticle monolayers of controlled coverage and structure, J. Phys. Chem. C 120 (22) (2016) 11807–11819, https://doi.org/10.1021/acs.jpcc.6b02683.
[34] Z. Adamczyk, Kinetics of diffusion-controlled adsorption of colloid particles and proteins, J. Colloid Interface Sci. 229 (2) (2000) 477–489, https://doi.org/10.1006/jcis.2000.6993.
[35] A. Bratek-Skicki, M. Sadowska, J. Maciejewska-Prończuk, Z. Adamczyk, Nanoparticle and bioparticle deposition kinetics: quartz microbalance measurements, Nanomaterials 11 (1) (2021) 145, https://doi.org/10.3390/nano11010145.
[36] P. Komorek, M. Wałek, B. Jachimska, Mechanism of lysozyme adsorption onto gold surface determined by quartz crystal microbalance and surface plasmon resonance, Bioelectrochemistry 135 (2020) 107582, https://doi.org/10.1016/j.bioelechem.2020.107582.
[37] M. Wasilewska, Z. Adamczyk, A. Pomorska, M. Nattich-Rak, M. Sadowska, Human serum albumin adsorption kinetics on silica: influence of protein solution stability, Langmuir 35 (7) (2019) 2639–2648, https://doi.org/10.1021/acs.langmuir.8b03266.
[38] K. Kubiak, Z. Adamczyk, M. Wasilewska, Mechanisms of fibrinogen adsorption at the silica substrate determined by QCM-D measurements, J. Colloid Interface Sci. 457 (2015) 378–387, https://doi.org/10.1016/j.jcis.2015.07.009.
[39] M. Wasilewska, P. Żeliszewska, K. Pogoda, P. Deptuła, R. Bucki, Z. Adamczyk, Human vimentin layers on solid substrates: adsorption kinetics and corona formation investigations, Biomacromolecules 23 (8) (2022) 3308–3317, https://doi.org/10.1021/acs.biomac.2c00415.
[40] H. Wei, Z. Wang, L. Yang, S. Tian, C. Hou, Y. Lu, Lysozyme-stabilized gold fluorescent cluster: synthesis and application as Hg2+ sensor, Analyst 135 (6) (2010) 1406–1410, https://doi.org/10.1039/C0AN00046A.

[41] B.A. Russell, B. Jachimska, P. Komorek, P.A. Mulheran, Y. Chen, Lysozyme encapsulated gold nanoclusters: effects of cluster synthesis on natural protein characteristics, Phys. Chem. Chem. Phys. 19 (10) (2017) 7228–7235, https://doi.org/10.1039/C7CP00540G.
[42] B. Jachimska, A. Kozłowska, A. Pajor-Swierzy, Protonation of lysozymes and its consequences for the adsorption onto a mica surface, Langmuir 28 (31) (2012) 11502–11510, https://doi.org/10.1021/la301558u.
[43] I. Hussain, S. Graham, Z. Wang, B. Tan, D.C. Sherrington, S.P. Rannard, A. I. Cooper, M. Brust, Size-controlled synthesis of near-monodisperse gold nanoparticles in the 1− 4 nm range using polymeric stabilizers, J. Am. Chem. Soc. 127 (47) (2005) 16398–16399, https://doi.org/10.1021/ja055321v.
[44] D. Ungor, A. Barbasz, A. Czyżowska, E. Csapó, M. Oćwieja, Cytotoxicity studies of protein-stabilized fluorescent gold nanoclusters on human lymphocytes, Colloids Surf. B Biointerfaces 200 (2021) 111593, https://doi.org/10.1016/j.colsurfb.2021.111593.
[45] A. Baksi, P.L. Xavier, K. Chaudhari, N. Goswami, S.K. Pal, T. Pradeep, Protein-encapsulated gold cluster aggregates: the case of lysozyme, Nanoscale 5 (5) (2013) 2009–2016, https://doi.org/10.1039/C2NR33180B.
[46] P.L. Xavier, K. Chaudhari, A. Baksi, T. Pradeep, Protein-protected luminescent noble metal quantum clusters: an emerging trend in atomic cluster nanoscience, Nano Rev. 3 (1) (2012) 14767, https://doi.org/10.3402/nano.v3i0.14767.
[47] U. Kreibig, P. Zacharias, Surface plasma resonances in small spherical silver and gold particles, Zeitschrift für Physik A Hadrons and nuclei 231 (2) (1970) 128–143, https://doi.org/10.1007/BF01392504.
[48] Y.H. Lin, W.L. Tseng, Ultrasensitive sensing of Hg2+ and CH3Hg+ based on the fluorescence quenching of lysozyme type VI-stabilized gold nanoclusters, Anal. Chem. 82 (22) (2010) 9194–9200, https://doi.org/10.1021/ac101427y.
[49] Z. Luo, X. Yuan, Y. Yu, Q. Zhang, D.T. Leong, J.Y. Lee, J. Xie, J. From aggregation-induced emission of Au (I)–thiolate complexes to ultrabright Au (0)@ Au (I)–thiolate core–shell nanoclusters, J. Am. Chem. Soc. 134 (40) (2012) 16662–16670, https://doi.org/10.1021/ja306199p.
[50] J. Luo, Z. Xie, J.W. Lam, L. Cheng, H. Chen, C. Qiu, B.Z. Tang, Aggregation-induced emission of 1-methyl-1, 2, 3, 4, 5-pentaphenylsilole, Chemical communications (18) (2001) 1740–1741, https://doi.org/10.1039/B105159H.
[51] T. Li, H. Zhu, Z. Wu, Viewing aggregation-induced emission of metal nanoclusters from design strategies to applications, Nanomaterials 13 (3) (2023) 470, https://doi.org/10.3390/nano1303047.
[52] Y. Tao, M. Li, J. Ren, X. Qu, Metal nanoclusters: novel probes for diagnostic and therapeutic applications, Chem. Soc. Rev. 44 (23) (2015) 8636–8663, https://doi.org/10.1039/C5CS00607D.
[53] M. Oćwieja, K. Matras-Postołek, J. Maciejewska-Prończuk, M. Morga, Z. Adamczyk, S. Sovinska, A. Żaba, M. Gajewska, T. Król, K. Cupiał, M. Bredol, Formation and stability of manganese-doped ZnS quantum dot monolayers determined by QCM-D and streaming potential measurements, J. Colloid Interface Sci. 503 (2017) 186–197, https://doi.org/10.1016/j.jcis.2017.04.059.
[54] A. Michna, Z. Adamczyk, P. Batys, Mapping single macromolecule chains using the colloid deposition method: PDADMAC on mica, J. Colloid Interface Sci. 450 (2015) 82–90, https://doi.org/10.1016/j.jcis.2015.02.057.
[55] Z. Adamczyk, M. Nattich-Rak, M. Dąbkowska, M. Kujda-Kruk, Albumin adsorption at solid substrates: a quest for a unified approach, J. Colloid Interface Sci. 514 (2018) 769–790, https://doi.org/10.1016/j.jcis.2017.11.083.
[56] M. Dąbkowska, Z. Adamczyk, Ionic strength effect in HSA adsorption on mica determined by streaming potential measurements, J. Colloid Interface Sci. 366 (1) (2012) 105–113, https://doi.org/10.1016/j.jcis.2011.09.030.
[57] Z. Adamczyk, A. Pomorska, M. Nattich-Rak, M. Wytrwal-Sarna, A. Bernasik, Protein adsorption mechanisms at rough surfaces: serum albumin at a gold substrate, J. Colloid Interface Sci. 530 (2018) 631–641, https://doi.org/10.1016/j.jcis.2018.06.063.